Anion Resonances of *para*-Benzoquinone Probed by Frequency-Resolved Photoelectron Imaging

*Christopher W. West, James N. Bull, Erkki Antonkov and Jan R. R. Verlet**

Department of Chemistry, Durham University, Durham, DH1 3LE

Corresponding Author

*j.r.r.verlet@durham.ac.uk

Abstract:

The resonant attachment of a free electron to a closed shell neutral molecule, and the interplay between the following electron detachment and electronic relaxation channels represents a fundamental but common process throughout chemical and biochemical systems. The new methodology of anion frequency-resolved photoelectron imaging is detailed and used to map-out molecular excited state dynamics of gas-phase *para*-benzoquinone, which is the electron accepting moiety in many biological electron-transfer chains. Three-dimensional spectra of excitation energy, electron kinetic energy and electron ejection anisotropy reveal clear fingerprints of excited and intermediate state dynamics. The results show that many of the excited states are strongly coupled, providing a route to forming the ground state radical anion, despite the fact that the electron is formally unbound in the excited states. The relation of our method to electron impact attachment studies and the key advantages, including the extension to time-resolved dynamics and to larger molecular systems is discussed.

KEYWORDS Resonances, Temporary negative ions, Quinone, Radical anions, Photoelectron spectroscopy, Photoelectron angular distributions.

Introduction

Electron transfer is amongst the most fundamental chemical reactions and features prominently in all branches of chemistry. Quinones are often encountered as part of the active site in electron transfer reactions in nature;[1-4] for example, plastoquinone and ubiquinone are key electron acceptors in the electron transport chains of photosynthesis[5] and respiration,[6] respectively. Inspired by their widespread use in nature, quinones have also been commonly used in synthetic electron transport chains in order to create simple prototypes that model the electron acceptor dynamics of these biological reaction centers.[7] Of the various quinone derivatives, the *para*-benzoquinone (pBQ) moiety is that most common in nature. From a rudimentary perspective, electron transfer to a closed shell neutral molecule such as pBQ can be viewed as the electron attachment through resonances of its radical anion. From this point-of-view, electron attachment and transmission studies on pBQ have attracted considerable interest over the last few decades.[8-14] Such studies have provided detailed insight into the available temporary anion resonances of pBQ, although dynamical information is typically difficult to extract because nascent excited state resonances can have lifetimes on a sub-picosecond timescale. We have recently shown that a photoelectron (PE) spectrum of $pBQ^{\bullet-}$ contains signatures of such ultrafast dynamics and that time-resolved PE spectroscopy can be used to follow these dynamics in real-time.[15] These time-resolved experiments considered excitation dynamics at a single photon energy (*hv*).

Here, we present a comprehensive study on the excitation energy or frequency-dependent PE imaging of $pBQ^{\bullet-}$ and show that PE spectral trends as well as the PE angular distributions (PADs) extracted from the PE images may be used to identify the location of excited state resonances, and that these show clear evidence for above-threshold dynamics involving several excited states of $pBQ^{\bullet-}$. The experimental methodology provides complementary and new

information concerning the analogous electron attachment processes. Moreover, frequency-resolved PE imaging can be readily scaled up to much larger and more complex system through the use of electrospray as a radical anion source, paving the way to studying the above-threshold dynamics of a range of important molecular systems.

The excited states of $pBQ^{\bullet-}$ have been the subject of a number of gas-phase [8-11,13-21] and computational[16,21-24] studies. It is well-established that both the radical anion and neutral pBQ have planar D_{2h} ground state geometries with $^2B_{2g}$ and ^1A_g electronic symmetry, respectively. Anion photodetachment experiments have determined the adiabatic electron affinity of pBQ to be 1.860 ± 0.005 eV.[16] By varying the photon energy, Schiedt and Weinkauf identified a number of vibrationally-resolved above-threshold resonances of jet-cooled $pBQ^{\bullet-}$.[16] Notably, a broad and intense peak at 2.50 eV above the anionic ground state was assigned to the ^2A_u excited state with predominantly shape resonance character. A series of weaker sharp resonances were assigned to vibrational states of the lower lying $^2B_{2u}$ and $^2B_{3g}$ states. Both of these are formally optically dark Feshbach resonances with predominantly $n\pi^*$ character, but they gain some oscillator strength due to Herzberg-Teller coupling with the ^2A_u state. Additionally, Schiedt and Weinkauf showed that the PE spectra at different excitation energies resonant with the ^2A_u state changed due to varying Franck-Condon factors following autodetachment. In another study, Wang and co-workers have reported PE spectra of $pBQ^{\bullet-}$ at ~70 K using 355 nm (3.496 eV) and 266 nm (4.661 eV) photons identifying no apparent vibrational structure for photon energies less than 4 eV, however at least two sharp spectral features with vibrational structure emerge at $h\nu$ ~4.2 eV.[21] Finally, Brauman and co-workers have reported low resolution *total* photodetachment cross sections with photon energies up to ~4.6 eV, identifying two broad maxima centered at ~3.0 eV and ~4.1 eV, as well as the onset of an intense band starting at ~4.4 eV.[25,26]

pBQ has also been the subject of a number of electron attachment and transmission studies, which have identified at least three resonances centered at 0.7 eV, 1.4 eV and ~2.0 eV above the ground state of the neutral, with the latter producing radical anions that survive for at least several microseconds.[8,12-14] Although some vibrational structure could be discerned in these experiments, on the whole, the bands are very broad and overlapping. In a number of other molecular systems, systematic electron attachment measurements have illustrated vibrationally-resolved two-dimensional electron attachment, which can be considered as analogous to the frequency-resolved methodology presented in this work.[27-29]

The experiments of Schiedt and Weinkauf demonstrated the sensitivity of PE spectroscopy to investigate excited state electron detachment processes of pBQ, although were limited to a narrow spectral range around the ^2A_u resonance and only changes in the vibrational structure were observed in the PE spectra. In this paper, we trade off spectral resolution for range and present PE spectra with $2.48 < h\nu < 4.59$ eV, thus probing up to 2.73 eV into the electron detachment continuum of $pBQ^{\bullet-}$. Furthermore, we employ angle resolved PE spectroscopy, which provides additional rich insight into resonances in the continuum. Comparison of anion PE spectra with neutral electron attachment and transmission spectra combined with high-level *ab initio* calculations on the energetics for appropriate geometries provides a comprehensive deconvolution of electron detachment dynamics.

Experimental

The experiment uses a velocity-map imaging PE spectrometer, combined with electrospray as an anion source. Details of the experiment have been presented elsewhere.[30-34] Briefly, $pBQ^{\bullet-}$ radical anions were produced by electrospray of ~1 mM of pBQ (97%, Sigma Aldrich) in

methanol, and trapped in a radio frequency ring-electrode ion trap operating at ambient temperature. Following unloading of the ion trap at a 10 Hz repetition rate, the ion packet was mass-separated by time-of-flight and $pBQ^{\bullet-}$ was irradiated at the center of a penetrating-field velocity-map-imaging assembly.[30,35] Laser pulses of ~6 ns duration with photon energies from 2.48 eV (500 nm) to 4.59 eV (270 nm) in 10 nm increments were generated using an optical parametric oscillator (Continuum Horizon I), which was pumped by a Nd:YAG laser (Continuum Surelite II-10). PE spectra and PADs were extracted from the raw images using a polar onion peeling algorithm.[36] The PE spectra were calibrated using the known spectrum of I^- and have a resolution of ~5 %.

Theoretical

Ab initio calculations were performed using the GAMESS-US (May 2013 release)[37] and Gaussian 09 computational packages.[38] All calculations used the aug-cc-pVTZ basis set to described the carbon and oxygen atoms, although the most diffuse set of *f* functions were omitted from this basis set.[39] The hydrogen atoms were described using the cc-pVTZ basis set.[40] The final molecular basis set should provide an accurate account of valence shells for shape or core-excited Feshbach resonances without excess diffuse mixing.[41] Following Weber *et al.*,[23] CASSCF reference wave functions with (16,12) and (17,12) active spaces for neutral and anion states, respectively, and were used for all geometrical optimizations and frequency calculations. All relevant zero-point energy corrections assumed harmonic values scaled with factor 0.98.[42] Dynamical electron correlation was added with MRMP2 theory, within the more general multi-state XMCQDPT framework.[43] The occurrence of intruder states in single state multi-reference calculations was checked by inspecting the weight of the reference function and applying

denominator level shifting. In some instances multistate calculations were performed to ensure level shifting was sufficient to remove any small intruder state contributions. Calculated ground state energetics (experimental values in parentheses) are AEA = 1.96 (1.86)[16] eV, VEA = 1.57 (1.5 ± 0.1)[14] eV, and VDE = 2.03 (2.0 ± 0.1)[21] eV, where AEA is the adiabatic electron affinity of pBQ, VEA is the vertical electron affinity of pBQ, and VDE is the vertical detachment energy of $pBQ^{\bullet -}$. For comparison, CCSD(T) theory[44] considering the same molecular basis set gives AEA = 1.85 eV, VEA = 1.63 eV, and VDE = 1.98 eV.

Results

Figure 1 shows three representative PE spectra taken at photon energies of: (a) 2.48 eV (500 nm); (b) 3.10 eV (400 nm); and (c) 4.13 eV (300 nm). The central slices through the respective reconstructed images are inset, where both the experimental (left) and Legendre polynomial fits are retained (right). The PE spectrum at 2.48 eV shows a main feature centered around an electron kinetic energy (*eKE*) of 0.4 eV. The maximum of this feature is consistent with that for a direct detachment process based on the 3.496 eV spectrum from the Wang group;[21] however, at *eKE* = 0 eV, an additional feature is observed that exponentially decays with increasing *eKE*. The PE spectrum at 3.10 eV is clearly more complicated. The feature centered at *eKE* ~0.9 eV is consistent with a direct detachment feature, but an additional feature can be seen around *eKE* ~0.4 eV as well as a peak at *eKE* = 0 eV. On initial inspection, the additional feature at *eKE* ~0.4 eV has the appearance of the PE spectrum recorded at 2.48 eV, but does not have the expected shift in *eKE* commensurate with the increase in photon energy for direct detachment – this trend becomes obvious in the two-dimensional spectrum. The 3.10 eV PE spectrum is essentially identical to our earlier spectrum acquired with laser pulses of ~40 fs duration,[15] implying that we

are observing single photon absorption despite the increase in the duration of the laser pulse to ~6 ns. The PE spectrum at 4.13 eV shows predominantly a single PE feature at high *eKE*, which is consistent with direct detachment and the additional feature observed in the 3.10 eV spectrum has essentially disappeared. A small peak at *eKE* = 0 eV can still be identified, although this is much weaker compared to the spectra at the other two photon energies.

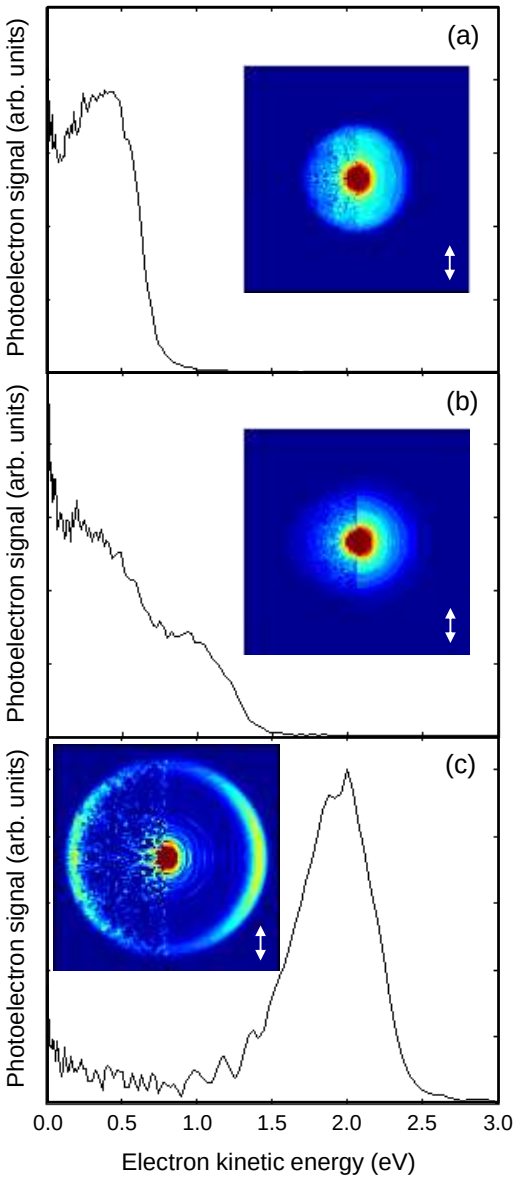

Figure 1: Photoelectron spectra acquired at photon energies of (a) 2.48 eV, (b) 3.10 eV, and (c) 4.13 eV. Inset in each plot are the central slices through the corresponding PE velocity-map image; the left semicircle is the experimental data retained in polar onion peeling and the right semicircle is the fitted Legendre polynomials.

To provide a complete overview for photon energies from 2.48 eV to 4.59 eV, the PE spectra are plotted in Figure 2 (a) and (b) in false-color. In Figure 2(a), each PE spectrum has been normalized to the relative total photoelectron cross sections of Brauman and co-workers.[25] The total integrated cross section increases rapidly for $h\nu > 3.8$ eV as evidenced by the prominence of the feature at high *eKE* in Figure 2(a). The cross section for direct detachment as a function of *eKE* is expected to be a smoothly increasing function and the sharp increase observed suggests that a resonance is accessed at these photon energies. At $h\nu > 4.2$ eV, a new feature emerges at low *eKE* which has been correlated with the excitation of excited states in the neutral following detachment.[21] The high *eKE* feature in this range scales linearly with photon energy as may be expected for a direct detachment PE feature. For $h\nu < 3.3$ eV, the PE spectra change quite dramatically indicative of processes occurring in the detachment continuum and therefore again pointing to resonances at these photon energies. However, the cross section in this energy range is significantly smaller than at higher photon energies.

To accentuate the spectral changes as a function of photon energy, in Figure 2(b), each PE spectrum has been normalized to the total area of that spectrum. This procedure illustrates that the *relative* intensities of PE features vary quite dramatically with excitation energy and clearly shows the changes in the PE spectra for $h\nu < 3.3$ eV. Specifically, at $eKE < 0.1$ eV, a maximum is observed for $h\nu \sim 2.9$ eV, and a second feature is observed in the $2.5 < h\nu < 3.3$ eV spectra that on first inspection seems to have a decreasing *eKE* with increasing photon energy. Finally, no resolvable vibrational structure was observed in any of these PE spectra.

In addition to the spectral changes observed as a function of excitation energy, clear changes can be observed in the PADs. The PADs are quantified by the anisotropy parameter (β_2) defined by the intensity as a function of the angle between PE ejection and laser polarization, $I(\theta)$:[45,46]

$$I(\theta) = \sigma\,(1 + \beta_2 P_2(\cos\theta)) / 4\pi,$$

where $P_2(\cos\theta)$ is the 2nd order Legendre polynomial and σ the total detachment cross section. The β_2 spectra in Figure 2(c) include a five-point moving average. Regions for which the PE signal is below 0.375 (area normalized intensity units), at which level the uncertainty in determining the PADs becomes very large, have been shaded out. The dashed diagonal line in figure 2 indicates the maximum *eKE* expected based on the known adiabatic electron affinity of 1.86 eV.

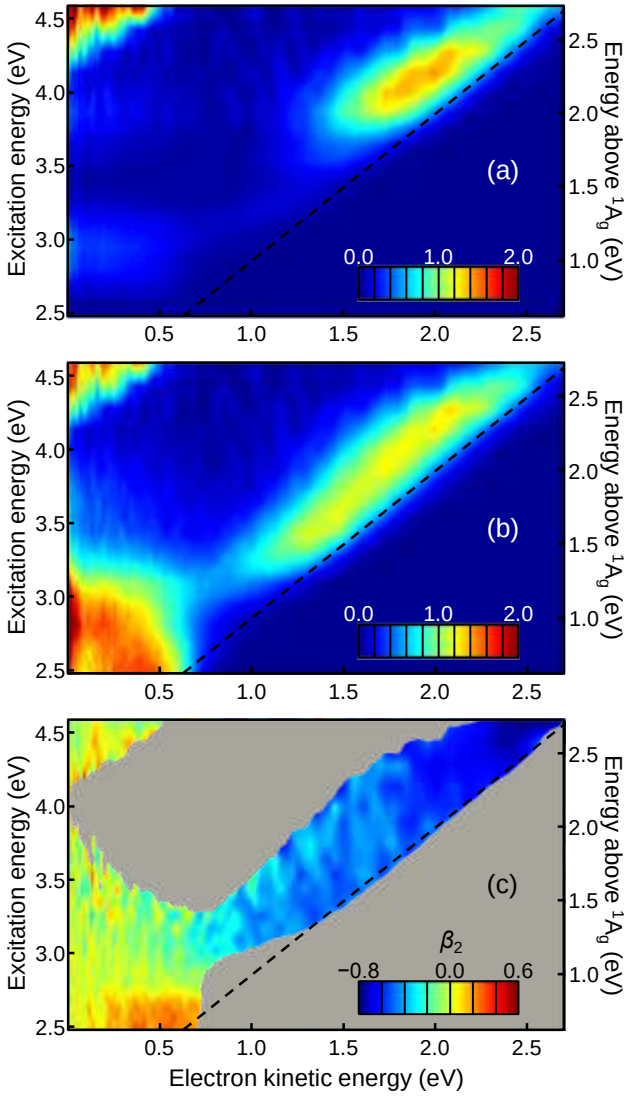

Figure 2: (a) Frequency-resolved photoelectron spectra normalized to the total detachment cross section; (b) same as (a), although normalized to the total integrated photoelectron signal in each spectrum; and (c) β_2 anisotropy parameter spectra as a function of excitation energy, where the shaded areas indicate regions with a normalized photoelectron intensity of less than 0.375. The dashed line indicates the maximum photoelectron kinetic energy available and the right-hand side axes indicate the energy above threshold.

Discussion

The PE signal in the lowest *eKE* window (< 0.1 eV) can be assigned to thermionic emission, corresponding to a statistical loss of electrons from hot vibrational ground state $pBQ^{\bullet-}$,[47-50] because the photodetachment cross section of an ideal anion falls to zero at threshold.[51,52] The broad peak centered around *eKE* ~0.4 eV is observed in all spectra with photon energies 2.5 < *hν* < 3.3 eV, although a small red-shift to *eKE* ~0.2 eV is observed around *hν* ~2.9 eV. Schiedt and Weinkauf have shown that at *hν* = 2.5 eV, the cross section to excitation of the ^2A_u shape resonance is significantly greater than direct detachment into the continuum. Hence, the feature at *eKE* ~0.4 eV can be assigned to autodetachment processes primarily from the ^2A_u shape resonance, with possible small contributions from the lower lying $^2B_{2u}$ Feshbach resonance. The calculated VDEs for autodetachment from the ^2A_u state to the ^1A_g state are 0.78 eV and 0.56 eV, considering $^2B_{2g}$ (anion ground state) and ^2A_u geometries, respectively. Detachment processes to higher vibrationally excited ^1A_g would shift these detachment distributions to lower *eKE*, however there have been no reports of resolved vibrational structure in this PE band. Additionally, the presence of a thermionic emission feature at *eKE* = 0 eV suggests that the anion ground state can be recovered following excitation to the ^2A_u state. An intermediate strength conical intersection between the ^2A_u and the slightly lower energy $^2B_{2u}$ state has been previously calculated,[15] which provides an internal conversion route between the two states. The small relative PE signal in the thermionic emission feature compared to the autodetachment peak (see Figure 2(b)) suggest, however, that the time-scale for internal conversion is longer. This would be in line with the fact that the ^2A_u state is a shape resonance and can thus be expected to lead to very fast autodetachment. Nevertheless, internal conversion can clearly compete as evidenced by the thermionic emission. In this process, the $^2B_{2u}$ (and possibly the $^2B_{3g}$) could be populated as

an intermediate, which may also undergo autodetachment and could therefore contribute to the PE spectra around $h\nu$ = 2.5 eV. The calculated VDE for the $^2B_{2u}$ state is 0.23 eV and 0.57 eV, assuming the $^2B_{2g}$ and ^2A_u geometries, respectively. Interestingly, the $^2B_{2u}$ Feshbach resonance in its equilibrium geometry is *bound* by around 0.52 eV. In fact, the calculated adiabatic detachment energy is also slightly negative at 0.06 eV, although this includes zero within the estimated ± 0.1 eV error inherent in these calculations.

The spectral features associated with the ^2A_u state persist for photon energies up to $h\nu$ ~3.3 eV, which are no longer resonant with the ^2A_u state. However, for 2.75 < $h\nu$ < 3.2 eV the *eKE* distribution shifts towards slightly lower *eKE* and is accompanied with a relative increase in the thermionic emission peak at *eKE* = 0 eV. The PADs clearly show that a new channel opens up at $h\nu$ = 2.75 eV. When $h\nu$ < 2.75 eV, β_2 = + 0.2 between 0.2 < *eKE* < 0.5 eV. This abruptly changes to β_2 = 0.0 between 2.75 < $h\nu$ < 3.2 eV over the same *eKE* range, while for *eKE* > 0.5 eV, β_2 is slightly negative. For a direct detachment process, gradual changes in anisotropy may be expected as partial waves with differing angular momentum interfere. Abrupt changes, as those observed here, point to sudden changes in the detachment process. At $h\nu$ = 2.5 eV, the excitation of the ^2A_u state leads to an alignment of the excited state ensemble, which may then undergo autodetachment on a timescale much faster than molecular rotation. The combination of alignment and the anisotropy expected for the autodetachment from the ^2A_u defines the observed PAD. This process persists up to $h\nu$ = 2.75 eV, where the anisotropy changes.

At $h\nu$ = 3.1 eV (400 nm), previous experiments and CASPT2 calculations have shown that the $(2)^2B_{3u}$ Feshbach resonance is excited and undergoes an internal conversion to the ^2A_u state on a ~20 fs timescale. This assignment is consistent with the spectra in Figures 1 (a) and (b), which both show autodetachment at *eKE* ~0.4 eV. Hence, a large part of the PE spectrum between 2.75

< $h\nu$ < 3.3 eV contains autodetachment from the ^2A_u state. The observation that the *eKE* of this autodetachment peak does not steadily increase with increasing photon energy suggests that the internal energy content of the ^2A_u (and $^2B_{2u}$) state is approximately conserved upon autodetachment into the $^1A_g + e^-$ continuum. Similar observations of non-shifting *eKE* features with $h\nu$ can be seen in the vibrational autodetachment from other anions[53,54] and in polyanions.[55-57] At first glance however, the abrupt change to $\beta_2 = 0.0$ for 2.75 < $h\nu$ < 3.2 eV is not consistent with the assignment of this peak to autodetachment from the ^2A_u state, as the same process is observed for $h\nu$ < 2.75 eV. However, the initially excited state for 2.75 < $h\nu$ < 3.2 eV is the $(2)^2B_{3u}$ state instead of the ^2A_u which is excited at $h\nu$ < 2.75 eV. This has a direct consequence as the transition dipole moments for excitation from the $^2B_{2g}$ ground state to the $(2)^2B_{3u}$ state and the ^2A_u state are orthogonal to each other. Hence, the initial $(2)^2B_{3u}$ excited state ensemble is aligned differently and, given that the internal conversion is much faster (~20 fs) compared to rotation, the autodetachment from the sequential ^2A_u state has a different laboratory-frame alignment. The abrupt changes in PADs around $h\nu$ = 2.75 eV might therefore be expected. At *eKE* > 0.5 eV, the anisotropy is negative and points to the fact that the higher energy peak of the PE spectrum (Figure 1(b)) corresponds to a different electronic state ($(2)^2B_{3u}$) than the peak around 0.4 eV (^2A_u), which provides additional support for our assignments.

In Figure 2(b), a maximum in the relative contribution of the thermionic emission peak (*eKE* = 0 eV) can be observed at $h\nu$ ~2.9 eV. This maximum is concomitant with a minimum in direct detachment and suggests that the internal conversion at this energy is most efficient; the thermionic peak must result from internal conversion to the $^2B_{2g}$ electronic ground state of the radical anion. This maximum also coincides with the first broad peak in the total relative detachment cross sections measured by Brauman and coworkers. The observed increase in

thermionic emission following excitation of the $(2)^2B_{3u}$ excited state relative to that following direct excitation of the ^2A_u state could occur through two mechanisms: (i) the $(2)^2B_{3u}$ state may undergo internal conversion directly to vibrationally hot $^2B_{2g}$ ground state; or (ii) the $(2)^2B_{3u}$ state may undergo internal conversion to a vibrationally excited ^2A_u, which in turn is able to undergo internal conversion (*via* the $^2B_{2u}$ state) to the $^2B_{2g}$ ground state more efficiently than the ^2A_u states produced by direct excitation. Calculations have identified a conical intersection that could funnel population directly into the $^2B_{2g}$ state, although requires a large out-of-plane motion, which was deemed unlikely based on the ~20 fs timescale of the internal conversion that was measured in time-resolved PE experiments.[15] The second mechanism, in which internal conversion to the ground state may be accelerated *via* internal conversion to the ^2A_u and $^2B_{2u}$ states, may thus be more likely. This latter mechanism would be promoted if the vibrational mode(s) coupling internal conversion out of the ^2A_u or $^2B_{2u}$ states are selectively excited following internal conversion from the $(2)^2B_{3u}$ state through the first conical intersection. Our calculations indicate that the $(2)^2B_{3u}$ geometry is more similar to the $^2B_{2u}$ state, while the $^2B_{2g}$ geometry is more similar to the ^2A_u state. Indeed, the PE spectrum following autodetachment for the two processes shows differences in the *eKE* distribution, as the local maximum shifts from 0.2 eV to 0.4 eV following preparation of the $^2A_u/^2B_{2u}$ state by internal conversion from the $(2)^2B_{3u}$ state or optical excitation, respectively (see figure 2(b)). It should also be noted that an additional conical intersection, also involving large out-of-plane motion, was identified between the ^2A_u and the $^2B_{2g}$ ground state that may only be accessible when large amounts of internal energy in the ^2A_u state are available and this may also explain the enhanced repopulation of the ground state to produce the thermionic emission peak.[15] Finally, we have also calculated a slightly lower-lying $(1)^2B_{3u}$ state, which has predominantly shape resonance character but it has a

negligible oscillator strength. In previous calculations, the ordering of these two $^2B_{3u}$ states was reversed because of the diffuse nature of the orbitals involved. As this $(1)^2B_{3u}$ state may be close in energy to the optically prepared $(2)^2B_{3u}$ state and of the same symmetry, it is not unreasonable to expect that this state may also play some role in the internal conversion dynamics from the excited $(2)^2B_{3u}$ state.

At $3.3 < h\nu < 4.2$ eV, figure 2(b) show the relative intensity of the constant *eKE* feature compared to the higher *eKE* features quickly diminishes with increasing photon energy. The higher *eKE* features shift with increasing photon energy as might be expected from a direct detachment process. However, the increase in total cross section in figure 2(a) for $h\nu > 3.5$ eV suggest an additional resonance in this energy range, which correlates with the broad shoulder centered at ~4 eV in the Brauman and co-workers photodetachment spectrum. The highest *eKE* feature does show evidence of a trend discontinuity at this energy, where the maximum of the peak has shifted to slightly lower *eKE*. Further, there remains a small thermionic contribution to the PE spectra, all implying either a broad absorption spectrum of the lowest $(2)^2B_{3u}$ Feshbach resonance or the appearance of a new channels correlating with the higher energy resonance. Finally, for $h\nu$ ~3.9 eV, PE features can be discerned in figure 2(a) with *eKE* < 0.5 eV that appear similar to those observed at lower excitation energy that were assigned to autodetachment from the ^2A_u state.

The most likely candidate for the observed increase in cross section at $h\nu > 3.5$ eV is an optically bright $(3)^2B_{3u}$ state. No other states with appreciable oscillator strength are located between this state and the $(2)^2B_{3u}$ state. The $(3)^2B_{3u}$ state has predominantly shape resonance character, which suggests that autodetachment is likely to be fast from this state. Nevertheless, one would anticipate some changes in the Franck-Condon envelope to the neutral ground state,

as observed by Schiedt and Weinkauf following ^2A_u autodetachment, which would account for the slight deviations in vertical binding energy of this peak around $h\nu \sim 4$ eV. Additionally, there is evidence for internal conversion to form intermediate states and the presence of thermionic emission at *eKE* = 0 eV. The relatively low yield of low energy electrons may be because of fast autodetachment or because internal conversion is not as efficient. The latter can be consolidated by the large energetic gap between the $(3)^2B_{3u}$ and lower excited states.

The PADs in the $3.5 < h\nu < 4.2$ eV vary monotonically from $\beta_2 = -0.5$ to -0.6, although the negative anisotropy is already evident at $h\nu = 3.0$ eV associated with autodetachment from the $(2)^2B_{3u}$ state. Given that the autodetachment is from a state of the same symmetry, it is not unreasonable to anticipate similar PADs for these two processes. Smooth variations with *eKE* are expected as the weighting of different partial waves are kinetic energy dependent.

At $h\nu = 4.2$ eV, new channels open that lead to the formation of neutral excited states. A number of states that these could correspond to have been identified and include the lowest lying $^3B_{1g}$, ^3A_u and $^1B_{1g}$, ^1A_u states.[41] Some of these states may be accessed directly from the ground state or may be formed following autodetachment from the $(3)^2B_{3u}$ state. In addition to the formation of excited neutral pBQ, there is evidence of thermionic emission reappearing for $h\nu >$ 4.2 eV. However, it is difficult to disentangle this from the intense features at low *eKE*. Our PE spectra do not show clear evidence for peaks that would identify intermediate states in this internal conversion process, although again, some of this may be obscured by the emergence of PE peaks leading to several different neutral excited states. The presence of the high *eKE* peak diminishes for $h\nu > 4.2$ eV, relative to the lower *eKE* peaks suggesting that the excitation is no longer resonant with the $(3)^2B_{3u}$ state at these energies. However, the cross section data of Brauman and co-workers indicates that an additional sharp increase in cross section is observed

for higher photon energies. Experimentally, it becomes difficult to measure high-quality PE spectra for photon energies above ~5 eV (250 nm) in the current set-up because laser flux from our OPO system rapidly decreases at shorter wavelengths and noise associated with the UV light increases.

The frequency-resolved PE energetics and interpretations can also be compared with literature electron transmission and attachment spectra.[58] The primary difference between these two techniques, aside from the two processes not complying to exactly the same selection rules,[59,60] is that they probe different initial geometries; PE spectroscopy initially prepares excited states assuming the geometry of the ground state anion, while electron attachment probes anion resonances from the neutral geometry. Moreover, it is generally observed in electron attachment experiments that shape resonances exhibit attachment cross sections up to several-fold larger than similar Feshbach resonances, which might be intuitively expected within the framework of Koopmans' theorem.[60] Similarly, autodetachment lifetimes for shape resonances are typically much faster than those of Feshbach resonances. In the limit of the anion and neutral geometries being similar (*i.e.* VEA ~VDE), the energetics produced from these two techniques should be comparable. For pBQ, the VEA and VDE differ by ~0.5 eV and our calculations indicate there are also changes in the relative energetics of several of the active resonances. Figure 3 summarises all calculated energies assuming the ^1A_g ground state neutral and $^2B_{2g}$ ground state anion equilibrium geometries, respectively.

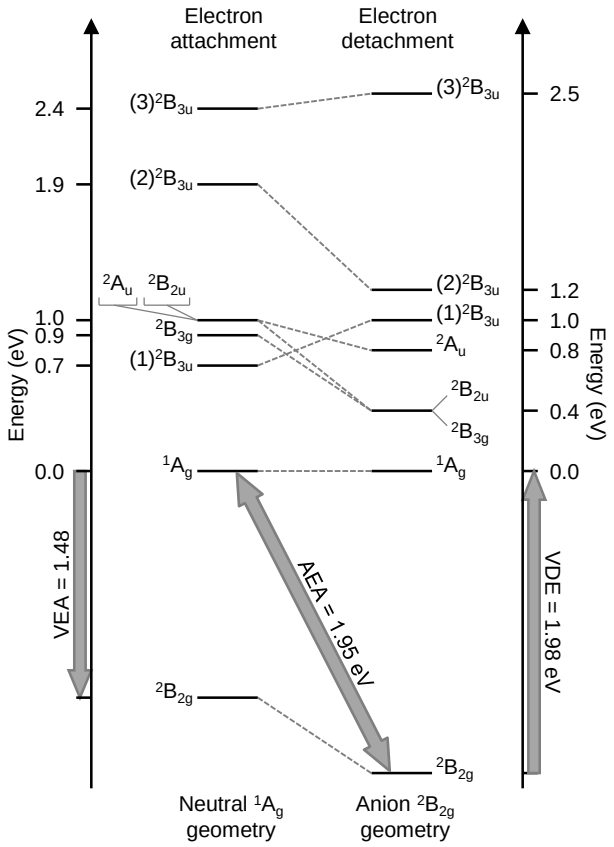

Figure 3: Calculated energy level diagram assuming ^1A_g neutral (left) and $^2B_{2g}$ anion (right) geometries. Energies given as vertical values with respect to the initial ground state; for the photoelectron case, the photon energy is given by adding the electron affinity.

Electron attachment spectra have indicated three low-energy resonances centred around 0.7 eV, 1.4 eV, and ~2.0 eV.[12-14] Of particular interest are the detailed experiments of Allan, identifying a number of specific vibrational excitations associated with several of these bands.[8,9] The electronic symmetry assignments of these three electron attachment resonances have been the subject of some controversy between different authors, primarily because assignments considered (erroneous) Koopmans' theorem energetics. Our calculations indicate that the 0.7 eV band probably corresponds with $(1)^2B_{3u}$ shape resonance calculated at 0.68 eV; the 1.4 eV band with the ^2A_u shape resonance calculated at 1.01 eV (and to some extent the $^2B_{2u}$ Feshbach resonance calculated at 1.03 eV); and the ~2.0 eV (weakest) band with the $(2)^2B_{3u}$ Feshbach resonance calculated to lie at 1.86 eV. The latter band may also have some contribution from the $(3)^2B_{3u}$ shape resonance, calculated at 2.4 eV.

In general, the electron attachment resonances are considerably broader than those from photoexcitation and detachment. Energetic agreement between the second 1.4 eV band and *ab initio* calculations is not ideal considering the very good agreement between all other calculated and experimental energies, and may indicate the involvement of some other processes. Of note, configuration interaction (SAC) calculations of Nakatsuji and co-workers[22], which have been considered as theoretical references in a number of experimental studies, have assignments of the $(1)^2B_{3u}$ and $(2)^2B_{3u}$ states reversed; overall the energetics calculated in this work are in significantly better agreement with experiment.

The electron attachment energetics can be compared with those for the associated PE experiments (Figure 3), with the most important change being the convergence of the two lowest $^2B_{3u}$ states within 0.2 eV of each other assuming the anion geometry. Optically, the $(1)^2B_{3u}$ is not directly accessible, although its participation in the dynamics *via* internal conversion cannot be

ruled out. The large separation in energy between the $(2)^2B_{3u}$ and $(3)^2B_{3u}$ states in the anion geometry is observed in Figure 2(a) as a region where direct detachment probably dominates the PE spectra. It is somewhat fortuitous that the PE spectra of the Wang group were collected at 3.496 eV and 4.661 eV, where the former lies within this gap such that the PE spectrum probably represents that without significant perturbations of autodetachment processes from resonances.

Finally, the time-resolved electron-energy-loss spectra of Allan assuming electron impact energies resonant with the band at ~2.0 eV or the $(2)^2B_{3u}$ Feshbach resonance, identified two detachment channels; a fast channel limited by the experimental resolution, and a much slower thermionic or so-called 'non-specific' vibrational excitation channel. These observations are in agreement with our earlier time-resolved PE measurements and the spectra recorded this work, in that efficient internal conversion and energy redistribution can produce a population of ground state anions that statistically detaches to the neutral. The fast channel can be correlated with autodetachment from the excited states. Similar to our PE spectra, the thermionic signal was also observed by Allan when the electron energy was tuned over the lower lying resonances, although this apparently occurred on shorter statistical detachment timescales than for the higher ~2.0 eV band. Further, Allan noted strong excitation of a few specific vibrations over the three resonances, which usually indicate a large change of equilibrium geometry. Apart from the lowest-lying $(1)^2B_{3u}$ shape resonance, it is indeed the case that for the $(2)^2B_{3u}$ Feshbach and ^2A_u shape resonances, the $^2B_{2g}$ anion geometry is closer to their equilibrium geometry than the ^1A_g neutral equilibrium geometry. It may therefore be that the lack of vibrational structure in our PE spectra compared with the electron attachment spectra is, in part, reflective of varying Frank-Condon factors.

In summary, the electron attachment spectra broadly agree with our frequency-resolved PE spectra, although the number of accessible states, and ultrafast dynamical timescales mean that detailed comparisons are difficult. The primary advantage of frequency-resolved PE imaging presented here is that the dynamics occurring on the excited states can be clearly identified through changes in the PE spectra as a function of excitation energy. In some respects, our methodology is analogous to two-dimensional electron impact studies, which to the best of our knowledge has only been demonstrated for electron attachment to N_2, CO_2 and C_3H_3N.[27-29] The additional dimension provided by the angular distributions in frequency resolved PE imaging offers even greater insight. As demonstrated here, the PADs can be very sensitive to changes in the symmetry of the resonances involved. Currently, only a qualitative discussion was offered. However, it should be possible to more formally calculate the differential electron ejection probability. This can be done by using, for example, the Dyson orbital approach, which works well for resonances in which only a single excitation dominates.[61,62] However, the calculation of PADs for more complex Feshbach resonance processes and autodetachment processes in general requires further theoretical input. The extension of anion PE imaging to the time-domain using femtosecond lasers allows the dynamics of very short-lived temporary negative ions to be studied in real-time and, combined with high-level *ab initio* calculations, ultimately provides the most detailed understanding of the dynamics. Finally, an important advantage of the frequency-resolved PE imaging approach presented here is that the range of systems that can be studied is almost infinite. Electrospray can be a very useful tool for generating a vast array of radical anions which can be used to probe the anionic resonances of the closed-shell neutral species.

Conclusions

Frequency-dependent photoelectron (PE) imaging to map-out resonances in the radical anion continuum can reveal excited state dynamics through both trends in the PE spectra and *via* anisotropies in the electron angular distributions. Changes in the PE spectra following the excitation of a resonance can be assigned to autodetachment from the prepared state that leads to changes in the Franck-Condon window to the final neutral states or internal conversion to lower lying states that subsequently autodetach. The additional information obtained through the PADs clearly identifies the involvement of resonances; similar changes in PADs have been observed in vibrational autodetachment of anions.[53,54] In principle, PADs can be calculated using, for example, the relevant Dyson orbitals.[61,62] However, when autodetachment occurs from resonances and interference can occur with direct detachment channels, these methods become more difficult to apply and additional development on the theoretical front is required to capture changes in the PADs.

The methodology presented in this paper can, in general, be applied to any system with a sufficiently positive adiabatic electron affinity to electrospray in good yield. Such processes are comparable with inelastic electron impact experiments and provide complementary information that enable the identification of above-threshold dynamics and the appearance of resonances. Electronic structure calculations and/or theoretical models are necessary to fully exploit the information provided by the frequency-resolved PE imaging, and this is particularly the case when there is a significant geometrical change between the ground states of the neutral and anion. As a final summary, frequency-resolved PE imaging has several key advantages over conventional electron attachment or transmission experiments: (i) the identification of intermediate electronic states with higher confidence; (ii) the addition of the angular electron ejection information; (iii) the ability to extend to the time-domain using femtosecond laser

sources allowing the dynamics to be probed in real-time; and (iv) anion preparation using electrospray can be easily applied to larger molecular systems that would be otherwise difficult to produce in the gas phase in abundant and stable number densities.

Notes

The authors declare no competing financial interests.

Acknowledgements

We are grateful to Gabrielle Lori for his assistance in these experiments and Daniel Horke for collecting the femtosecond PE spectra. Funding was provided by the ERC under Starting Grant 306536 and the EPSRC.

Supporting Information

All photoelectron spectra comprised in the two-dimensional spectrum (Figure 1b). This material is available free of charge via the Internet at http://pubs.acs.org.

References

(1) El-Najjar, N.; Gali-Muhtasib, H.; Ketola, R. A.; Vuorela, P.; Urtti, A.; Vuorela, H. *Phytochem. Rev.* **2011**, *10*, 353.

(2) Nohl, H.; Jordan, W.; Youngman, R. J. *Adv. Free Rad. Biol. Med.* **1986**, *2*, 211.

(3) Brunmark, A.; Cadenas, E. *Free Rad. Biol. Med.* **1989**, *7*, 435.

(4) Closs, G. L.; Miller, J. R. *Science* **1988**, *240*, 440.

(5) Kurisu, G.; Zhang, H.; Smith, J. L.; Cramer, W. A. *Science* **2003**, *302*, 1009.

(6) Iverson, T. M.; Luna-Chavez, C.; Cecchini, G.; Rees, D. C. *Science* **1999**, *284*, 1961.

(7) Fukuzumi, S. *Bull. Chem. Soc. Japan* **2006**, *79*, 177.

(8) Allan, M. *Chem. Phys.* **1983**, *81*, 235.

(9) Allan, M. *Chem. Phys.* **1984**, *84*, 311.

(10) Modelli, A.; Burrow, P. D. *Journal of Physical Chemistry* **1984**, *88*, 3550.

(11) Strode, K. S.; Grimsrud, E. P. *Chem. Phys. Lett.* **1994**, *229*, 551.

(12) Christophorou, L. G.; Carter, J. G.; Christodoulides, A. A. *Chem. Phys. Lett.* **1969**, *3*, 237.

(13) Collins, P. M.; Christophorou, L. G.; Chaney, E. L.; Carter, J. G. *Chem. Phys. Lett.* **1970**, *4*, 646.

(14) Cooper, C. D.; Naff, W. T.; Compton, R. N. *J. Chem. Phys.* **1975**, *63*, 2752.

(15) Horke, D. A.; Li, Q.; Blancafort, L.; Verlet, J. R. R. *Nature Chem.* **2013**, *5*, 711.

(16) Schiedt, J.; Weinkauf, R. *J. Chem. Phys.* **1999**, *110*, 304.

(17) Pshenichnyuk, S. A.; Asfandiarov, N. L.; Fal'ko, V. S.; Lukin, V. G. *Int. J. Mass Spectrom.* **2003**, *227*, 281.

(18) Asfandiarov, N. L.; Pshenichnyuk, S. A.; Fokin, A. I.; Nafikova, E. P. *Chem. Phys.* **2004**, *298*, 263.

(19) El Ghazaly, M. O. A.; Svendsen, A.; Bluhme, H.; Nielsen, S. B.; Andersen, L. H. *Chem. Phys. Lett.* **2005**, *405*, 278.

(20) Siegert, S.; Vogeler, F.; Weinkauf, R. *Zeit. Phys. Chem.* **2011**, *225*, 507.

(21) Fu, Q.; Yang, J.; Wang, X.-B. *J. Phys. Chem. A* **2011**, *115*, 3201.

(22) Honda, Y.; Hada, M.; Ehara, M.; Nakatsuji, H. *J. Phys. Chem. A* **2002**, *106*, 3838.

(23) Weber, J.; Malsch, K.; Hohlneicher, G. *Chem. Phys.* **2001**, *264*, 275.

(24) Pou-Amerigo, R.; Serrano-Andres, L.; Merchan, M.; Orti, E.; Forsberg, N. *J. Am. Chem. Soc.* **2000**, *122*, 6067.

(25) Comita, P. B.; Brauman, J. I. *J. Am. Chem. Soc.* **1987**, *109*, 7591.

(26) Marks, J.; Comita, P. B.; Brauman, J. I. *J. Am. Chem. Soc.* **1985**, *107*, 3718.

(27) Regeta, K.; Allan, M. *Phys. Rev. Lett.* **2013**, *110*, 203201.

(28) Currell, F.; Comer, J. *Phys. Rev. Lett.* **1995**, *74*, 1319.

(29) Reddish, T.; Currell, F.; Comer, J. *J. Phys. E: Sci. Instrum.* **1988**, *21*, 203.

(30) Horke, D. A.; Roberts, G. M.; Lecointre, J.; Verlet, J. R. R. *Rev. Sci. Instrum.* **2012**, *83*, 063101.

(31) Lecointre, J.; Roberts, G. M.; Horke, D. A.; Verlet, J. R. R. *J. Phys. Chem. A* **2010**, *114*, 11216.

(32) Chatterley, A. S.; Horke, D. A.; Verlet, J. R. R. *Phys. Chem. Chem. Phys.* **2012**, *14*, 16155.

(33) Horke, D. A.; Chatterley, A. S.; Verlet, J. R. R. *J. Phys. Chem. Lett.* **2012**, *3*, 834.

(34) Horke, D. A.; Verlet, J. R. R. *Phys. Chem. Chem. Phys.* **2011**, *13*, 19546.

(35) Eppink, A. T. J. B.; Parker, D. H. *Rev. Sci. Instrum.* **1997**, *68*, 3477.

(36) Roberts, G. M.; Nixon, J. L.; Lecointre, J.; Wrede, E.; Verlet, J. R. R. *Rev. Sci. Instrum.* **2009**, *80*, 053104.

(37) Schmidt, M. W.; Baldridge, K. K.; Boatz, J. A.; Elbert, S. T.; Gordon, M. S.; Jensen, J. H.; Koseki, S.; Matsunaga, N.; Nguyen, K. A.; Su, S. J.; Windus, T. L.; Dupuis, M.; Montgomery, J. A. *J. Comput. Chem.* **1993**, *14*, 1347.

(38) Frisch, M. J.; Trucks, G. W.; Schlegel, H. B.; Scuseria, G. E.; Robb, M. A.; Cheeseman, J. R.; Scalmani, G.; Barone, V.; Mennucci, B.; Petersson, G. A.; Nakatsuji, H.; Caricato, M.; Li, X.; Hratchian, H. P.; Izmaylov, A. F.; Bloino, J.; Zheng, G.; Sonnenberg, J. L.; Hada, M.; Ehara, M.; Toyota, K.; Fukuda, R.; Hasegawa, J.; Ishida, M.; Nakajima, T.; Honda, Y.; Kitao, O.; Nakai, H.; Vreven, T.; Montgomery Jr., J. A.; Peralta, J. E.; Ogliaro, F.; Bearpark, M. J.; Heyd, J.; Brothers, E. N.; Kudin, K. N.; Staroverov, V. N.; Kobayashi, R.; Normand, J.; Raghavachari, K.; Rendell, A. P.; Burant, J. C.; Iyengar, S. S.; Tomasi, J.; Cossi, M.; Rega, N.; Millam, N. J.; Klene, M.; Knox, J. E.; Cross, J. B.; Bakken, V.; Adamo, C.; Jaramillo, J.; Gomperts, R.; Stratmann, R. E.; Yazyev, O.; Austin, A. J.; Cammi, R.; Pomelli, C.; Ochterski, J. W.; Martin, R. L.; Morokuma, K.; Zakrzewski, V. G.; Voth, G. A.; Salvador, P.; Dannenberg, J. J.; Dapprich, S.; Daniels, A. D.; Farkas, Ö.; Foresman, J. B.; Ortiz, J. V.; Cioslowski, J.; Fox, D. J.; Gaussian, Inc.: Wallingford, CT, USA, 2009.

(39) Kendall, R. A.; Dunning Jr., T. H.; Harrison, R. J. *J. Chem. Phys.* **1992**, *96*, 6796.

(40) Dunning Jr., T. H. *J. Chem. Phys.* **1989**, *90*, 1007.

(41) Schreiber, M.; Silva-Junior, M. R.; Sauer, S. P. A.; Thiel, W. *J. Chem. Phys.* **2008**, *128*.

(42) Merrick, J. P.; Moran, D.; Radom, L. *J. Phys. Chem. A* **2007**, *111*, 11683.

(43) Granovsky, A. A. *J. Chem. Phys.* **2011**, *134*, 214113.

(44) Pople, J. A.; Head-Gordon, M.; Raghavachari, K. *J. Chem. Phys.* **1987**, *87*, 5968.

(45) Zare, R. N. *Mol. Photochem.* **1972**, *4*, 1.

(46) Sanov, A. *Ann. Rev. Phys. Chem.* **2014**, *65*, 341.

(47) Amrein, A.; Simpson, R.; Hackett, P. *J. Chem. Phys.* **1991**, *94*, 4663.

(48) Amrein, A.; Simpson, R.; Hackett, P. *J. Chem. Phys.* **1991**, *95*, 1781.

(49) Baguenard, B.; Pinare, J. C.; Bordas, C.; Broyer, M. *Phys. Rev. A* **2001**, *63*.

(50) Andersen, J. U.; Bonderup, E.; Hansen, K. *J. Phys. B: At. Mol. Opt. Phys.* **2002**, *35*, R1.

(51) Pegg, D. J. *Rep. Prog. Phys.* **2004**, *67*, 857.

(52) Wigner, E. P. *Phys. Rev.* **1948**, *73*, 1002.

(53) Schneider, H.; Vogelhuber, K. M.; Schinle, F.; Stanton, J. F.; Weber, J. M. *J. Phys. Chem. A* **2008**, *112*, 7498.

(54) Mbaiwa, F.; Wei, J.; Van Duzor, M.; Mabbs, R. *J. Chem. Phys.* **2010**, *132*, 134304.

(55) Xing, X.-P.; Wang, X.-B.; Wang, L.-S. *J. Phys. Chem. A* **2010**, *114*, 4524.

(56) Butcher, C. P. G.; Johnson, B. F. G.; McIndoe, J. S.; Yang, X.; Wang, X.-B.; Wang, L.-S. *J. Chem. Phys.* **2002**, *116*, 6560.

(57) Horke, D. A.; Chatterley, A. S.; Verlet, J. R. R. *J. Chem. Phys.* **2013**, *139*, 084302.

(58) Jordan, K. D.; Burrow, P. D. *Chem. Rev.* **1987**, *87*, 557.

(59) Goddard III, W. A.; Huestis, D. L.; Cartwright, D. C.; Trajmar, S. *Chem. Phys. Lett.* **1971**, *11*, 329.

(60) Allan, M. *Helv. Chim. Acta* **1982**, *65*, 2008.

(61) Oana, C. M.; Krylov, A. I. *J. Chem. Phys.* **2007**, *127*, 234106.

(62) Oana, C. M.; Krylov, A. I. *J. Chem. Phys.* **2009**, *131*, 124114.